

# Brownian Dynamics Study of Diffusiophoretically Self-Propelled Colloidal Particle Near a Planar Wall

Ali Mozaffari,<sup>1</sup> Nima Sharifi-Mood,<sup>2</sup> Joel Koplik,<sup>3, a)</sup> and Charles Maldarelli<sup>1, b)</sup>

<sup>1)</sup>*Benjamin Levich Institute and Department of Chemical Engineering,  
City College of the City University of New York, New York, NY 10031,  
USA*

<sup>2)</sup>*CD-adapco - A Siemens Business, Lebanon, NH 03766,  
USA*

<sup>3)</sup>*Benjamin Levich Institute and Department of Physics,  
City College of the City University of New York, NY 10031,  
USA*

(Dated: 9 December 2024)

Under suitable conditions, a colloidal particle moving due to self-induced diffusiophoresis near a planar wall can exhibit skimming or stationary states of motion, in which the particle maintains a fixed distance from the wall. Such configurations have been found theoretically in the deterministic limit of the mass transfer and Stokes equations and here we examine their stability. We first demonstrate linear hydrodynamic stability by expanding the equations of motion about the stationary state, and find that linear perturbations decay exponentially in time. We then explicitly study the effects of thermal fluctuations within the context of Langevin dynamics, adding appropriate fluctuation and drift terms and solving the resulting stochastic differential equations numerically. Consistent with the stability results, the skimming and stationary states are found to persist with modest fluctuations at high Péclet number but become unstable at lower values. We present representative individual trajectories along with probability distributions for statistical ensembles of particles, quantifying the effects of thermal fluctuations.

---

<sup>a)</sup>Electronic mail: jkoplik@ccny.cuny.edu.

<sup>b)</sup>Electronic mail: cmaldarelli@ccny.cuny.edu.

## I. INTRODUCTION

The autonomous self-induced motion of colloidal particles<sup>1-3</sup> has received extensive recent attention, driven in large measure by possible applications in areas such as drug delivery, cargo transport, and lab-on-a-chip platforms<sup>4-7</sup>. A popular and well-studied example of the requisite propulsion mechanism is self-diffusiophoresis<sup>8-10</sup>. These swimmers are fabricated as a particle with partial coating of catalyst where the consumption of fuel in the surrounding fluid due to catalytic reaction on a subregion of a particle's surface drives the particle motion.

Diffusiophoretic self-propulsion which is the focus of present study originates from tangential surface gradient of solute concentration around the colloid surface. Short range interaction of electrically neutral product solute with colloid generates slip velocity at the outer edge of colloid surface which is proportional to surface gradient of solute concentration<sup>11</sup>. So, the concentration gradient is imperative for propulsion of particle which is usually obtained by chemically patterning the surface of particle (Janus). It also has been shown that uniformly coated catalytic colloids are able to move<sup>12,13</sup> for example due to geometric asymmetry<sup>14</sup> or curvature variation along the surface of motor<sup>15</sup>. Several theoretical works have used continuum framework of phoretic motion, based on slip model<sup>8</sup>, to address the dynamic of self propelled colloid in the stokes flow limit for example the effect of solute advection<sup>16,17</sup> and simple shear flow<sup>18</sup> on swimming velocity of janus microswimmer.

In an unbound fluid and in the absence of any perturbation such a particle moves in a straight line, and a particle approaching a wall is most likely to collide or reflect away from it. However, in many of the foreseen applications it is desirable for the colloid to remain in the close proximity to a specific delivery region or site, typically located along a wall bounding a mobile fluid region such as a microfluidic channel or blood vessel. Several recent experiments<sup>19-22</sup> and calculations<sup>23-27</sup> have addressed this issue, and have focused on particle trajectories which lead to more favorable behavior. In particular, conditions on the initial velocity and orientation of a particle approaching a wall have been obtained which lead to "skimming" states in which the particle moves parallel to the wall at small separations, and even stationary states in which the particle simply sits next to a wall. These calculations consider only deterministic motion, based on solutions of the continuum mass transfer equations for the catalytic reactants and the Stokes equations for fluid and particle motion in an otherwise uniform environment. In any realistic situation, other particles or contaminants

or mechanical perturbations will be present and the hydrodynamic stability of the skimming and stationary trajectories is an issue. Furthermore, and more generally, colloidal particles exhibit Brownian motion due to thermal fluctuations in the fluid environment which may obliterate deterministic motion<sup>28-30</sup>. Intuitively, one expects Brownian effects to dominate for small or slow particles or high temperature, but more quantitative results are needed in diffusiophoretic applications. Brownian dynamics of simple active brownian particles (subject to constant propulsion force and without hydrodynamic interactions) has been studied<sup>31</sup> for isotropic and anisotropic particles and also for the collection of two dimensional micro-rods near a V shaped solid wall<sup>32</sup>. Theoretical and experimental analysis of brownian motion of chemically powered janus swimmer<sup>9</sup> revealed the transition from initial directed motion to diffusive regime at longer time. The effect of brownian motion on the trapping time of self propelled bi-segmented Au-Pt rod and also squirmers (pushers and pullers) which orbits around passive spherical particle and the comparison of swimming through colloidal crystal for E. coli bacteria and catalytic janus swimmer has been studied<sup>33-35</sup>. The effect of thermal fluctuations on the distribution of detention time of active brownian particles and also squirmers near a planar no-slip wall<sup>36</sup> is theoretically studied.

In this paper we examine the stability issues for skimming and stationary self-diffusiophoretic particle motion. The calculations closely follow the deterministic analysis in our previous paper<sup>26</sup>, where the instantaneous solutions of the governing equations give the linear and angular velocity at each particle position and orientation, which are used to update the configuration by a time-stepping procedure. We first consider the hydrodynamic stability of solutions to the continuum equations, and the result is that they are indeed linearly stable. We then focus on Brownian motion; here the deterministic configuration update is augmented by fluctuation and drift terms<sup>37</sup>, and modified trajectories result. The key parameter is the Péclet number, defined precisely below but roughly the ratio of diffusiophoretic kinetic energy to thermal energy  $k_B T$ . At high Péclet number the deterministic behavior is preserved, but with non-growing fluctuations, whereas in the opposite limit skimming and stationary behavior could be lost completely.

## II. FORMULATION AND ANALYTICAL SOLUTION

### A. Langevin Equation

At the continuum level, a colloidal particle moving in a fluid is subject to deterministic forces  $\mathbf{F}_P$ , hydrodynamic forces  $\mathbf{F}_H$ , and fluctuating Brownian forces  $\mathbf{F}_B$ , which represent the effects of (unresolved) sub-micron scale atomic interactions with fluid molecules. The equation of motion is the Langevin stochastic differential equation<sup>38</sup>:

$$\mathbf{m} \frac{d\mathbf{V}}{dt} = \mathbf{F}_H + \mathbf{F}_P + \mathbf{F}_B, \quad (1)$$

where  $\mathbf{V}$  is a vector of translational and angular velocities and  $\mathbf{m}$  is a diagonal matrix whose elements are the particle's mass and moment of inertia. In low Reynolds number flow the hydrodynamic force can be written as  $\mathbf{F}_H = \mathfrak{R} \cdot \mathbf{u}$ , where  $\mathfrak{R}$  is a resistance matrix, and the Brownian force is characterized by its moments,

$$\langle \mathbf{F}_B(t) \rangle = 0, \quad (2)$$

$$\langle \mathbf{F}_B(t) \mathbf{F}_B(t') \rangle = 2k_B T \mathfrak{R} \delta(t - t'), \quad (3)$$

where  $\langle \cdot \rangle$  denotes an ensemble average,  $k_B$  is Boltzmann's constant and  $T$  is the fluid temperature. Eq. 3, which relates the strength of Brownian and hydrodynamic forces, is a consequence of the fluctuation-dissipation theorem and ensures that the system is in local thermodynamic equilibrium. In the present problem the deterministic forces arise from diffusiophoresis, and since the particle and the bounding wall are the only solids present, the resistance matrix is a function of the distance to the wall alone.

### B. Diffusiophoresis force and torque

The force driving the motion of a colloid is the interaction with the solute concentration gradient around the surface, so the first step is to solve the mass transfer equation for the solute. In the limit of small solute Péclet number, the advection of solute can be neglected and if the reaction rate is negligible compared to the solute diffusion rate (small Damköhler number) we may assume a uniform solute production rate ( $N_0$ ) at the active face of colloid (and zero flux at the passive face). The governing equation and boundary conditions can

then be written, in dimensionless form, as:

$$\nabla^2 C = 0, \quad (4)$$

$$\mathbf{n} \cdot \nabla C = 0, \quad \mathbf{r} \in \Gamma_W, \quad (5)$$

$$-\mathbf{n} \cdot \nabla C = \begin{cases} 1 & \mathbf{r} \in \Gamma_{AP} \\ 0 & \mathbf{r} \in \Gamma_{PP} \end{cases}, \quad (6)$$

$$C \rightarrow 0, \quad |\mathbf{r}| \rightarrow \infty, \quad (7)$$

Here  $\Gamma_W$ ,  $\Gamma_{AP}$  and  $\Gamma_{PP}$  represent the surfaces of the wall, the active side of particle and the passive part of particle, respectively. The solute concentration  $C(\mathbf{r})$  has been non-dimensionalized as  $C = \tilde{C}(N_0 a/D_s)^{-1}$ , where  $a$  is particle radius and  $D_s$  is the solute diffusivity, and  $\nabla = a\tilde{\nabla}$ . The active cap geometry is specified by the coverage angle  $\theta_{cap}$  and the tilt angle  $\Xi$  and the remaining parameter is the gap distance  $\delta$  between the particle and the wall, nondimensionalized by  $a$ . We solve for the solute concentration using the three-dimensional solution of Laplace's equation in bispherical coordinate.

The concentration couples to the fluid flow through the diffusiophoretic slip velocity boundary condition on the particle surface,  $\tilde{v}_s = -b\tilde{\nabla}_s\tilde{C}$ . At low Reynolds number the Stokes and continuity equations apply, and their dimensionless form is

$$\nabla^2 \mathbf{v} - \nabla p = 0, \quad (8)$$

$$\nabla \cdot \mathbf{v} = 0, \quad (9)$$

subject to the following boundary conditions

$$\mathbf{v} = -\nabla_s C, \quad \mathbf{r} \in \Gamma_P, \quad (10)$$

$$\mathbf{v} = 0, \quad \mathbf{r} \in \Gamma_W, \quad (11)$$

$$\mathbf{v} = 0, \quad |\mathbf{r}| \rightarrow \infty, \quad (12)$$

where  $\mathbf{v} = \tilde{\mathbf{v}}/\tilde{v}_c$ ,  $p = \tilde{p}(\mu\tilde{v}_c/a)^{-1}$  and  $\tilde{v}_c = bN_0/D_s$ . The mobility coefficient  $b$  in the boundary condition is defined as

$$b = (k_B T L^2/\mu) \int_0^\infty dy y [\exp(-\phi/k_B T) - 1],$$

where  $\phi$  is the solute/colloid interaction potential,  $L$  is its range and  $y$  is the distance to the surface of particle. The traction of the flow field at the particle surface produces the

diffusiophoretic force and torque via

$$\tilde{\mathbf{F}}_P = \oint_{\Gamma_P} (\tilde{\boldsymbol{\sigma}} \cdot \mathbf{n}) ds, \quad (13)$$

$$\tilde{\mathbf{T}}_P = \oint_{\Gamma_P} (\mathbf{r}_p - \mathbf{r}_o) \times (\tilde{\boldsymbol{\sigma}} \cdot \mathbf{n}) ds. \quad (14)$$

Here,  $\tilde{\boldsymbol{\sigma}} = -\tilde{p}\mathbf{I} + \mu [\nabla\tilde{\mathbf{v}} + (\nabla\tilde{\mathbf{v}})^T]$  is stress tensor,  $\mathbf{n}$  is the outward unit vector normal to the particle surface  $\Gamma_P$ , and  $\mathbf{r}$  and  $\mathbf{r}_o$  are position vectors on the particle surface and at the particle's center of mass, respectively. For a given cap geometry, the magnitudes of the diffusiophoretic force and torque are functions of the tilt angle and gap distance to the wall, and their orientations are as follows. If the unit vector  $\hat{\mathbf{u}}$  specifies the orientation of the particle, e.g., a vector pointing from the center of the particle to the center of the cap, and  $\hat{\mathbf{n}}_W$  is the unit vector normal to the wall, then the force is in the plane formed by these two vectors and the torques is in the direction of  $\hat{\mathbf{n}}_W \times \hat{\mathbf{u}}$ . In Cartesian coordinates where the wall is the  $x$ - $y$  plane,  $\tilde{\mathbf{T}}_{Pz} = 0$  at all times.

### C. Hydrodynamics Force and Torque

For a sphere near a plane wall the resistance matrix takes the form

$$\tilde{\mathfrak{R}} = \pi\mu a \begin{pmatrix} 6f_{\parallel}^{tt} & 0 & 0 & 0 & -6af_{\parallel}^{rt} & 0 \\ 0 & 6f_{\parallel}^{tt} & 0 & 6af_{\parallel}^{rt} & 0 & 0 \\ 0 & 0 & 6f_{\perp}^{tt} & 0 & 0 & 0 \\ 0 & 8af_{\parallel}^{tr} & 0 & 8a^2f_{\parallel}^{rr} & 0 & 0 \\ -8af_{\parallel}^{tr} & 0 & 0 & 0 & 8a^2f_{\parallel}^{rr} & 0 \\ 0 & 0 & 0 & 0 & 0 & 8a^2f_{\perp}^{rr} \end{pmatrix}, \quad (15)$$

where the subscripts  $\parallel$  and  $\perp$  refer to motion parallel and perpendicular to the wall, respectively, and the superscripts  $tt$ ,  $rr$ ,  $rt$ ,  $tr$  represent translation, rotation and the coupling between translation and rotation. The components of resistance matrix are functions of the dimensionless gap distance  $\delta$ , to be found. The linearity of the Stokes equations allows us to decompose the latter problem into four independent sub-problems:

- Translation of a sphere perpendicular to the wall gives  $f_{\perp}^{tt}$ .

- Translation of a non-rotating sphere parallel to the wall gives  $f_{\parallel}^{tt}$  and  $f_{\parallel}^{tr}$ .
- Rotation of a non-translating sphere around axis parallel to the wall gives  $f_{\parallel}^{rr}$  and  $f_{\parallel}^{rt}$ .
- Rotation of a sphere around an axis normal to the wall gives  $f_{\perp}^{rr}$ .

The details of solution for each resistance problem can be found in our previous paper<sup>26</sup>, except for the last problem which is discussed in the Appendix 1.

#### D. Linear Stability Analysis

We<sup>26</sup> and others<sup>25</sup> have shown that (in the absence of Brownian motion) a diffusiophoretically active colloid, at a certain inclination angle  $\Xi$  and coverage  $\theta_{cap}$ , can skim along a wall<sup>26</sup> and can arrive at a completely stationary state at suitably high values of the coverage. The objective of this section is to examine the stability of the skimming and stationary states with respect to small perturbations.

The dynamics of the system in the deterministic limit is governed by a set of first order differential equations

$$\frac{d\mathbf{x}}{dt} = \mathbf{U}(\mathbf{x}, \mathbf{n}_p), \quad \frac{d\mathbf{n}_p}{dt} = \mathbf{\Omega}(\mathbf{x}, \mathbf{n}_p), \quad (16)$$

where  $\mathbf{x}$  is the location of the colloid's center of mass,  $\mathbf{n}_p$  is a unit vector fixed in the particle which specifies its orientation, and the functions  $\mathbf{U}$  and  $\mathbf{\Omega}$  are given in<sup>26</sup>. If  $\mathbf{x}^*$  and  $\mathbf{n}_p^*$  specify a critical point, we can expand the equations about this point to leading order:

$$\begin{aligned} \frac{d\mathbf{x}}{dt} &= \mathbf{U}|_{\mathbf{x}^*, \mathbf{n}_p^*} + (\mathbf{x} - \mathbf{x}^*) \cdot \nabla_{\mathbf{x}} \mathbf{U}|_{\mathbf{x}^*, \mathbf{n}_p^*} + (\mathbf{n}_p - \mathbf{n}_p^*) \cdot \nabla_{\mathbf{n}_p} \mathbf{U}|_{\mathbf{x}^*, \mathbf{n}_p^*}, \\ \frac{d\mathbf{n}_p}{dt} &= \mathbf{\Omega}|_{\mathbf{x}^*, \mathbf{n}_p^*} + (\mathbf{x} - \mathbf{x}^*) \cdot \nabla_{\mathbf{x}} \mathbf{\Omega}|_{\mathbf{x}^*, \mathbf{n}_p^*} + (\mathbf{n}_p - \mathbf{n}_p^*) \cdot \nabla_{\mathbf{n}_p} \mathbf{\Omega}|_{\mathbf{x}^*, \mathbf{n}_p^*}. \end{aligned} \quad (17)$$

In terms of Cartesian coordinates we can write  $\delta\mathbf{x} \equiv \mathbf{x} - \mathbf{x}^* = \sum_{i=1}^3 dx_i \mathbf{e}_i$ , and likewise  $\delta\mathbf{n}_p \equiv \mathbf{n}_p - \mathbf{n}_p^* = \sum_{i=1}^3 d\varphi_i \mathbf{e}_i$ , so that the above equations (ignoring the inhomogeneous constant terms as they do not have a role in stability analysis) take the form

$$\begin{aligned} \frac{d}{dt} \delta\mathbf{x} &= \mathbf{J}_1^* \cdot \delta\mathbf{x} + \mathbf{J}_3^* \cdot \delta\mathbf{n}_p, \\ \frac{d}{dt} \delta\mathbf{n}_p &= \mathbf{J}_2^* \cdot \delta\mathbf{x} + \mathbf{J}_4^* \cdot \delta\mathbf{n}_p, \end{aligned} \quad (18)$$

in terms of the  $3 \times 3$  matrices

$$\begin{aligned} \mathbf{J}_1^* &= \left( \frac{\partial U_i}{\partial x_j} \right) \Big|_{\mathbf{x}^*, \mathbf{n}_p^*}, & \mathbf{J}_3^* &= \left( \frac{\partial U_i}{\partial \varphi_j} \right) \Big|_{\mathbf{x}^*, \mathbf{n}_p^*}, \\ \mathbf{J}_2^* &= \left( \frac{\partial \Omega_i}{\partial x_j} \right) \Big|_{\mathbf{x}^*, \mathbf{n}_p^*}, & \mathbf{J}_4^* &= \left( \frac{\partial \Omega_i}{\partial \varphi_j} \right) \Big|_{\mathbf{x}^*, \mathbf{n}_p^*}, \end{aligned}$$

where the asterisk denotes the derivatives are being evaluated at the critical point. The equations given in (18) are linear differential equations with constant coefficients, and the stability of the stationary point is controlled by the eigenvalues of the grand Jacobian matrix

$$\mathbf{J}^* = \begin{pmatrix} \mathbf{J}_1^* & \mathbf{J}_3^* \\ \mathbf{J}_2^* & \mathbf{J}_4^* \end{pmatrix}. \quad (19)$$

Generally, a critical point of a system of differential equations is stable if all the eigenvalues of the grand Jacobian evaluated at the stationary point have negative real parts, unstable if at least one of the eigenvalues has a positive real part and marginally stable if one or more eigenvalues are zero and the others are negative<sup>39</sup>. In this problem, there are three zero eigenvalues because the swimming particle's dynamics are indifferent with respect to translations in the plane of the wall and rotations about the normal to the wall. More specifically, for a given active coverage  $\theta_{cap}$ , the swimming particle's translational  $\mathbf{U}$  and angular  $\mathbf{\Omega}$  velocities depend only on the distance  $\delta$  between the particle and the wall and its inclination angle  $\Xi$ , but do not depend on  $x$  and  $y$ , and hence the first two columns of the grand Jacobian matrix are identically zero. The system is also invariant under rotations about the  $z$  axis and consequently the system contains three zero eigenvalues and at best is marginally stable.

In evaluating  $\mathbf{J}^*$  for stationary state, we assume the orientation vector of the colloid is initially in the  $x - z$  plane and  $\Xi = 180^\circ$ . We then perturb the location of particle center of mass and its orientation vector infinitesimally in all directions,  $|\delta \mathbf{x}| \sim 0.01 - 0.1$  and  $|\delta \mathbf{n}_p| \sim 1^\circ$ , we then calculate the partial derivatives utilizing a central finite difference scheme. For each (sufficiently large) particle coverage  $\theta_{cap}$ , there is a unique separation distance  $\delta^*$  where the colloid is stationary, and in Table I we present the eigenvalues of  $\mathbf{J}^*$  for various colloid coverages at the appropriate  $\delta^*$ . Aside from the expected three zero values, the eigenvalues are real and negative for all coverages. Notice once the particle is in stationary state, it's inclination angle is precisely perpendicular to both  $x$  and  $y$  axes ( $\Xi = 180^\circ$ ) and inasmuch as the magnitudes of imposed angular perturbations around these

axes are identical, the corresponding eigenvalues (see  $\lambda_2$  and  $\lambda_5$  in Table I) for the two modes are exactly identical.

$\theta_{cap}$	$\delta^*$	$\Xi$	$\lambda_1$	$\lambda_2$	$\lambda_3$	$\lambda_4$	$\lambda_5$	$\lambda_6$
145°	0.065	180°	0.0	-0.0085	-0.1448	0.0	-0.0085	0.0
147°	0.18	180°	0.0	-0.0619	-0.1611	0.0	-0.0619	0.0
150°	0.38	180°	0.0	-0.0433	-0.1550	0.0	-0.0433	0.0
152°	0.55	180°	0.0	-0.0242	-0.1030	0.0	-0.0242	0.0
155°	0.84	180°	0.0	-0.0147	-0.1146	0.0	-0.0147	0.0
160°	1.50	180°	0.0	-0.0060	-0.7032	0.0	-0.0060	0.0
162°	1.85	180°	0.0	-0.0032	-0.0273	0.0	-0.0032	0.0
165°	2.55	180°	0.0	-0.0010	-0.2650	0.0	-0.0010	0.0

TABLE I. Eigenvalues of the grand Jacobian matrix for stationary state for various colloid coverages.

A similar analysis can be performed for the skimming state. Here, the inclination angles  $\Xi$  are no longer identical in all cases and they depend on the particle coverage and hence the three non-zero eigenvalues are distinct. In Table II we present the eigenvalues of  $\mathbf{J}^*$  for various colloid coverages at the critical point. The magnitude of perturbations for skimming state were chosen to be  $|\delta\mathbf{x}| \sim 0.01 - 0.06$  and  $|\delta\mathbf{n}_p| \sim 3 - 5^\circ$ . Here, for cases where  $\theta_{cap} > 120^\circ$ , two eigenvalues correspond to perturbation for translation along the  $z$  axis and rotation around the  $y$  axis are complex conjugate numbers but the real part of them are all negative and thus they are stable points. These points are so called “spiral” stable points as their solution trajectories in the  $z - \Xi$  plane tend to spiral around the critical point before they are merged into it.

## E. Brownian Dynamics Algorithm

Following standard methods<sup>37</sup>, when the Langevin equation can be twice integrated over time to yield a stochastic differential equation for the particle displacements in the over-damped limit:

$$\Delta\tilde{\mathbf{x}} = \tilde{\mathbf{M}} \cdot \tilde{\mathbf{F}}_P \Delta\tilde{t} + k_B T \tilde{\nabla} \cdot \tilde{\mathbf{M}} \Delta\tilde{t} + \sqrt{2k_B T} \tilde{\mathbf{B}} \cdot \Delta\tilde{\mathbf{w}}, \quad (20)$$

$\theta_{cap}$	$\delta^*$	$\Xi$	$\lambda_1$	$\lambda_2$	$\lambda_3$	$\lambda_4$	$\lambda_5$	$\lambda_6$
115°	0.359	123.4°	0.0	-0.0272	-0.2659	0.0	-0.0001	0.0
120°	0.243	132.8°	0.0	-0.0826	-0.2933	0.0	$-8.86 \times 10^{-5}$	0.0
125°	0.177	141.0°	0.0	$-0.2047 - 0.0751 i$	$-0.2047 + 0.0751 i$	0.0	-0.0001	0.0
130°	0.133	148.7°	0.0	$-0.1987 - 0.1847 i$	$-0.1987 + 0.1847 i$	0.0	-0.0003	0.0
135°	0.102	156.3°	0.0	$-0.1708 - 0.2492 i$	$-0.1708 + 0.2492 i$	0.0	-0.0009	0.0
142°	0.071	168.5°	0.0	$-0.1023 - 0.2035 i$	$-0.1023 + 0.2035 i$	0.0	-0.0025	0.0

TABLE II. Eigenvalues of the grand Jacobian matrix for skimming state for various colloid coverages and notice  $i = \sqrt{-1}$ .

where  $\tilde{\mathbf{x}}$  is a six-dimensional vector of particle translational and angular displacements,  $\tilde{\mathbf{M}} = \tilde{\mathfrak{R}}^{-1}$  is the mobility matrix and  $\tilde{\mathbf{B}}$  is a lower triangle matrix satisfying  $\tilde{\mathbf{B}} \cdot \tilde{\mathbf{B}}^T = \tilde{\mathbf{M}}$  which can be obtained from a Cholesky decomposition of  $\tilde{\mathbf{M}}$ . The last term involves  $\Delta\tilde{\mathbf{w}}$ , an Wiener process whose first and second moments are  $\langle \Delta\tilde{\mathbf{w}} \rangle = \mathbf{0}$  and  $\langle \Delta\tilde{w}_i \Delta\tilde{w}_j \rangle = \delta_{ij} \Delta\tilde{t}$ , in practice six independent Gaussian random numbers. The equation is written in the Ito convention where the mobility matrix elements and forces/torques are computed at the beginning of each time step.

In this case since rotations about different axes do not commute, care is needed when the particle's orientation is updated and we employ an unbiased rotational moves algorithm<sup>40</sup>. (This reference contains a typographical error – the (2,2) element of the transformation matrix Eq. 5 should read  $[(\Omega_a^2 + \Omega_c^2) \cos \Omega + \Omega_b^2]/\Omega^2$ .) The mobility is a function only of the distance to the wall and becomes constant at large separation, so the second “drift” term on the right hand side of Eq. 21 (which arises in the passage to the overdamped limit) has only a  $z$ -component and acts to push particles away from the wall<sup>41</sup>. This term appears from the  $f_{\perp}^{tt}$  entry of the resistance matrix, and its contribution to the equation of motion is illustrated in Fig. 1.

Lastly, for the numerical computations we write the evolution equation Eq. 20 in dimensionless form as

$$\Delta\mathbf{x} = Pe (\mathfrak{R}^{-1} \cdot \mathbf{F}_P \Delta t) + \nabla \cdot \mathfrak{R}^{-1} \Delta t + \sqrt{2} \mathbf{B} \cdot \Delta\mathbf{w}, \quad (21)$$

where the colloid Péclet number is defined as  $Pe = \pi\mu a^2 \tilde{v}_c / k_B T$ . In this equation,  $\mathbf{x} = \tilde{\mathbf{x}}/a$ ,  $\Delta t = \Delta\tilde{t}/t^*$ , and  $\Delta\mathbf{w} = \Delta\tilde{\mathbf{w}}/\sqrt{t^*}$  where  $t^* = \pi\mu a^3 / k_B T$  is the rotational diffusion time. In

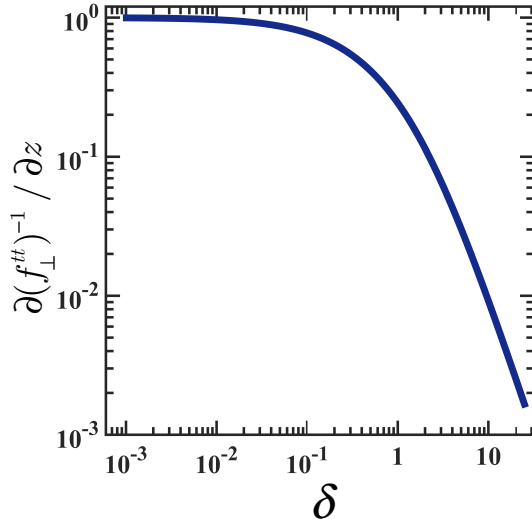


FIG. 1. Thermal drift term

$\mathbf{F}_P$  the force and torque entries are non-dimensionalized with  $\pi\mu a\tilde{v}_c$  and  $\pi\mu a^2\tilde{v}_c$  respectively, and  $\mathbf{B} \cdot \mathbf{B}^T = \Re^{-1}$ .

### III. RESULTS

In previous work<sup>25,26</sup> in the absence of Brownian forces, corresponding to the limit  $Pe \rightarrow \infty$ , the general nature of the trajectory of a particle near the wall was related to the initial orientation and the angular coverage of the active cap. If the initial orientation is normal to the wall and the cap faces the wall, the accumulation of solute in the gap drives the particle away, whereas if the cap is on the outward side the particle moves towards the wall. The particle does not reach the wall (in finite time) because of hydrodynamic interactions: fluid must be expelled from the gap and a lubrication flow occurs. For general initial orientations, the particle translates in the plane formed by the orientation axis and the wall normal, while rotating about an axis parallel to the cross product of the latter two vectors. Independent of the coverage, when  $\Xi < 90^\circ$  the particle is repelled from the wall for the same reason as above, but for larger  $\Xi$  the solute build up on the outward side initially drives the particle towards the wall. If the coverage is not too large ( $\theta_{cap} < 115^\circ$ ), the particle scatters from the wall while for a range of higher coverage  $115^\circ < \theta_{cap} < 145^\circ$  the particle skims along the wall at a constant separation  $\delta_{eq}$  with constant orientation  $\Xi_{eq}$ . For very high coverage  $\theta_{cap} > 145^\circ$  the particle moves to a stationary state very near the wall with zero translational

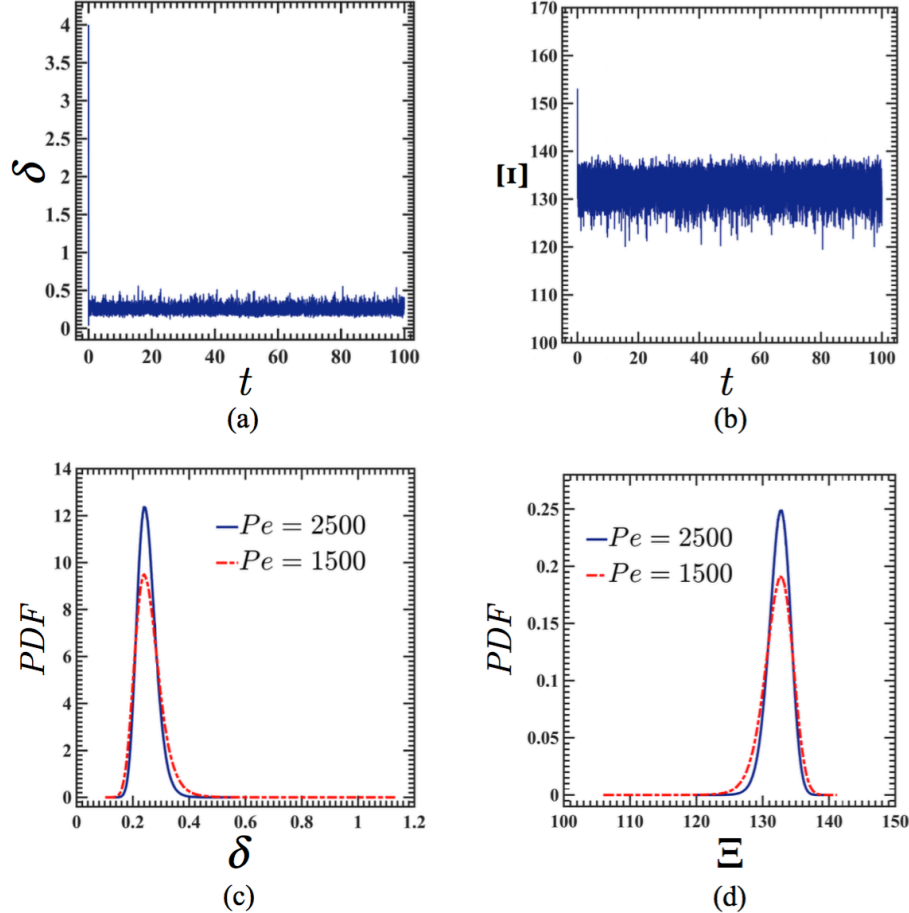


FIG. 2. Swimmer with  $\theta_{cap} = 120^\circ$  and initial configuration  $\delta = 4.0$  and  $\Xi = 150^\circ$  at  $Pe = 1500$ . (a) Variation of gap with time, (b) variation of tilt angle with time (single realization), (c) Probability distribution of gaps for  $Pe = 1500$  and  $2500$ , (d) Probability distributions of tilt angle (obtained from a very long time simulation).

and angular velocity and fixed orientation  $\Xi_{eq} = 180^\circ$ . The skimming and stationary states have potential applications in cargo transport and mixing, and in the following discussion we focus on their sensitivity to Brownian thermal fluctuations.

### A. Skimming swimmers

Normally at high Péclet number,  $Pe > 1000$  say, one expects small fluctuations about a deterministic trajectory but here small changes in orientation can have drastic effects on the motion. As shown in Fig. 2, the gap and the tilt angle  $\Xi$  are quite stable in this limit, with probability distributions that peak sharply about the deterministic values  $\delta_{eq} = 0.22$

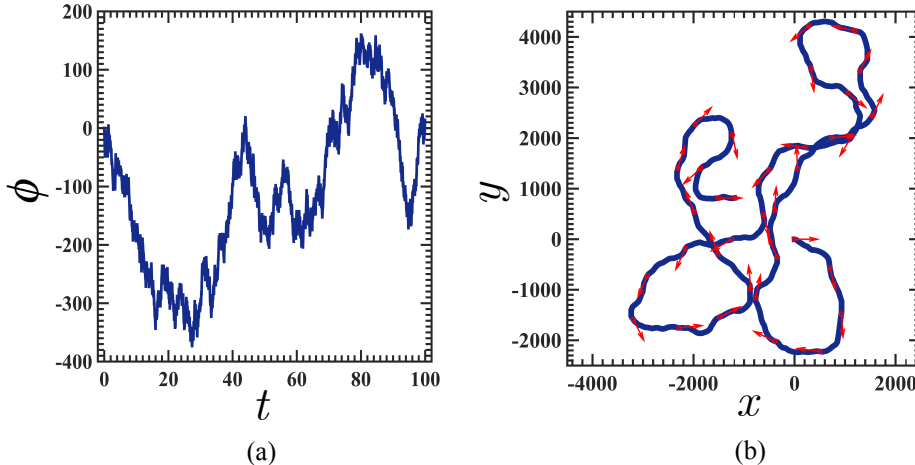


FIG. 3. Same swimmer as in Fig. 2. (a) Variation of the in-plane orientation angle  $\phi$  with time, (b) Trajectory in the  $x$ - $y$  plane. The red arrows represent the projection of orientation vector of particle on the  $x$ - $y$  plane.

and  $\Xi_{eq} = 133^\circ$  while broadening as  $Pe$  decreases. The fact that  $\Xi$  is stable is a necessary requirement for skimming at nearly-constant  $\delta$ . However, there are also fluctuations in  $\phi$ , the angle the projection of the orientation onto the wall makes with the  $x$ -axis, so that the orientation vector moves along a noisy circle about  $\Xi_{eq}$  on the unit sphere. The result in a torque about the  $z$ -axis which causes the direction of motion to fluctuate – see Fig. 3 – resulting in a persistent random walk in the  $x$ - $y$  plane.

When the Péclet number decreases further the fluctuations in tilt and gap become more pronounced, and only transient skimming states are observed once  $Pe < 200$ . Two typical trajectories are given in Fig. 4, the second illustrating the possibility of a particle skimming, leaving the wall region, and returning to skim in a different direction.

A useful characterization of the skimming states is the persistence time, the interval over which skimming persists, as a function of Péclet number. The average time is not the most suitable measure since the calculations have a time limit and in some cases skimming does not terminate, so instead we give the probability distributions of skimming time for different (moderate) values of  $Pe$  in Fig. 5. More precisely, we define the skimming time as the first passage interval between a particle reaching  $\delta_{eq}$  and  $\delta_{eq} + 1$ . We have also used other criteria such as the time at which the tilt angle becomes less than  $90^\circ$  but the results have the same trends and general behavior. We have seen in the figure that as the Péclet number increases

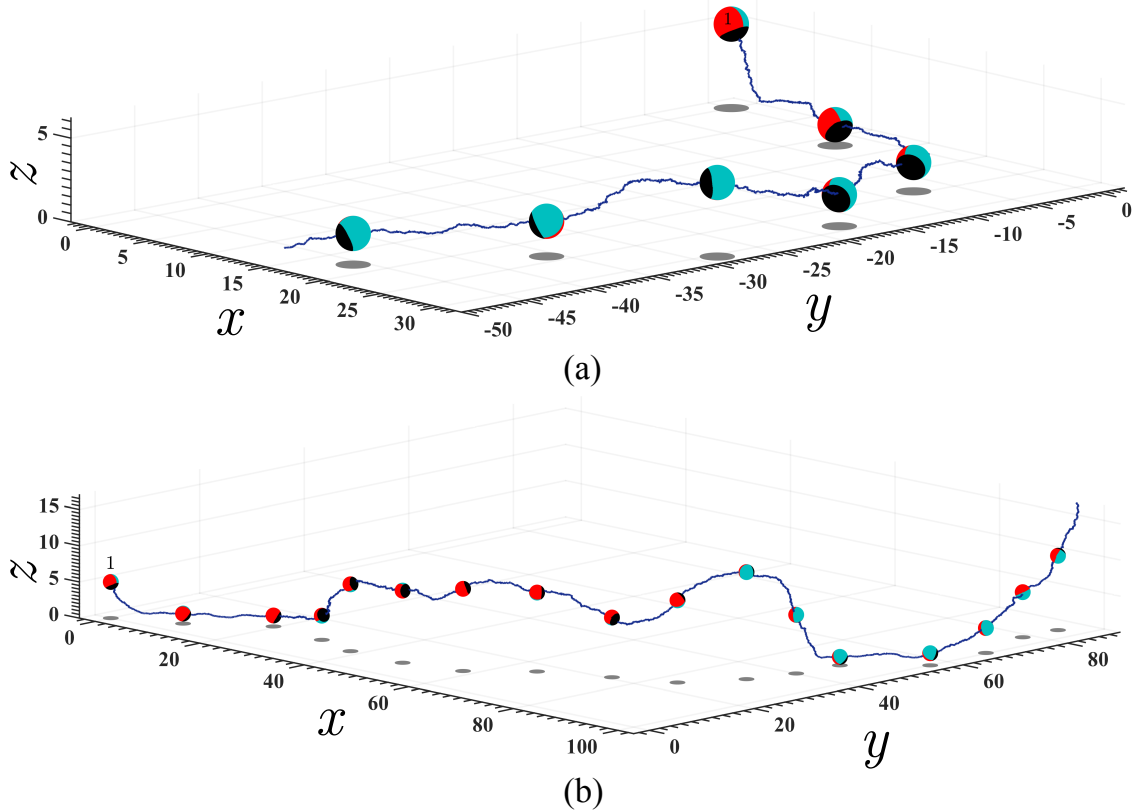


FIG. 4. Two sample trajectories for swimmer with  $\theta_{cap} = 120^\circ$  and an initial configuration  $\delta = 4.0$ ,  $\Xi = 150^\circ$  for  $Pe = 50$ . The black color shows the passive part. The active side represented by red and light blue colors to better show the rotation.

the skimming time distribution shifts toward longer values, and by  $Pe = 700$  most of the particles do not leave the plane for the duration of the simulation.

We wish to further analyze the in-plane random motion of the skimmers, in the limit of high  $Pe = 1500$  where skimming is persistent. We first compare the mean-square displacement (MSD) of a such skimmer to hypothetical skimmer which moves purely in two dimensions at the deterministic equilibrium values of gap and tilt ( $\delta_{eq}$ ,  $\Xi_{eq}$ ) but with rotational thermal noise acting on the particle only in the  $z$ -direction, and also to  $2/3$  of the MSD of an unconfined three-dimensional swimmer. We see in Fig. 6a that in all cases there is a transition from ballistic to diffusive motion at times distinctly longer than the rotational diffusion time, and that in the latter regime the three situations have distinctly different diffusivities (slopes). The difference between the purely two and three dimensional swimmers is that in 2d the orientation vector moves on a unit circle and decays exponentially with

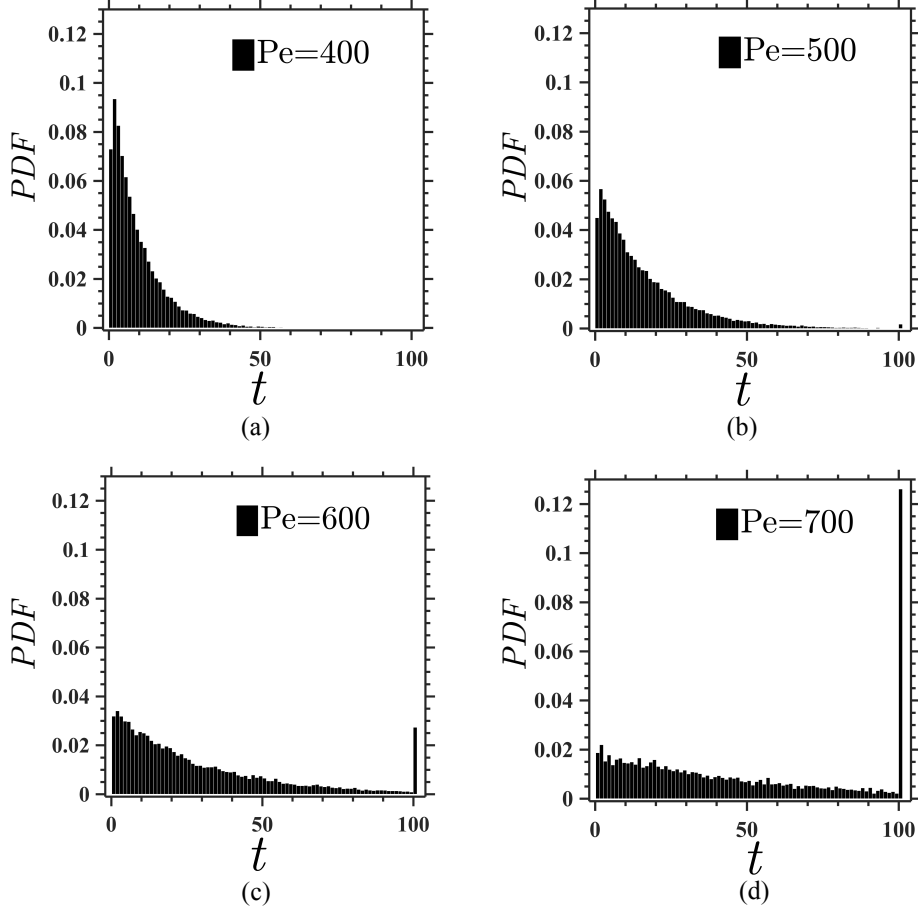


FIG. 5. Probability distribution of skimming time for four different values of the Péclet number.

time as  $\langle \hat{u}(t) \cdot \hat{u}(0) \rangle = \exp(-D_R t)$ , slower than a 3d swimmer where the orientation vector is diffuses on the unit sphere with correlation function decaying as  $\langle \hat{u}(t) \cdot \hat{u}(0) \rangle = \exp(-2D_R t)$  (see Appendix 2). The orientation of the 2d skimmer remains correlated for a longer time so uni-directional motion is more persistent. The simulated swimmer is in between since its orientation vector is not completely free to diffuse on the unit sphere but has more freedom in comparison with the 2d skimmer. A similar trend is apparent in Fig. 6b which compares the average displacement along the initial skimming direction  $\langle x(t) - x(0) \rangle$  for purely 2d skimmers and the simulated swimmer. In both cases, rotational diffusion eventually randomizes the direction of motion, but in the former case the particle moves further on average since its orientation is more persistent. A similar comparison can be made for the average  $y$ -displacements but more interestingly the probability distributions for simulated swimmers, Fig. 7, shows non-Gaussian behavior initially, followed by a transition to a Gaussian shape

at long times in the diffusive regime.

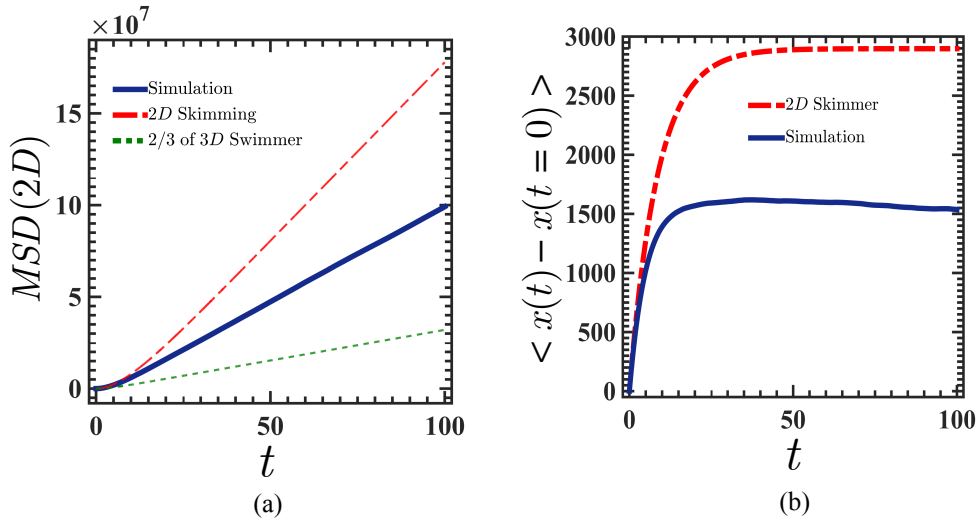


FIG. 6. Moments of the particle displacement at  $Pe = 1500$ . (a) Mean square displacement for the simulated swimmer (blue), 2d skimmer (red) and a swimmer in an infinite medium (green). (b) Average  $x$ -position of the simulated swimmer and the 2d skimmer.

## B. Stationary swimmers

In the absence of thermal fluctuations, a particle with very high coverage  $\theta_{cap} > 145^\circ$  and initial orientation away from the wall comes to a stop at the equilibrium gap distance  $\delta_{eq}$  and an orientation normal to the wall  $\Xi_{eq} = 180^\circ$ . When the Péclet number is large,  $Pe > 1000$ , this remains a stable state: the gap and orientation fluctuate about the deterministic values, as shown in Fig. 8 for a typical example. Fluctuations in  $\delta$  are weak because the stationary position is an attractor due to the opposing propulsion and lubrication forces there. Fluctuations in  $\Xi$  produce a force parallel to the wall which is resisted by lateral hydrodynamic drag, resulting in somewhat larger motions parallel to the wall. The in-plane rotation is in random directions due to fluctuations in  $\phi$  which are unsurpassed because the deterministic forces does not give torque about the  $z$ -axis. Going beyond this single example, Fig. 9 shows the lateral motions for five sample realizations at  $Pe = 1500$ , along with the probability distribution functions of gap and inclination angle.

We can characterize the diffusive motion by the mean square displacement, shown in Fig. 10a, which indicates an effective diffusivity much greater than that of an ordinary two

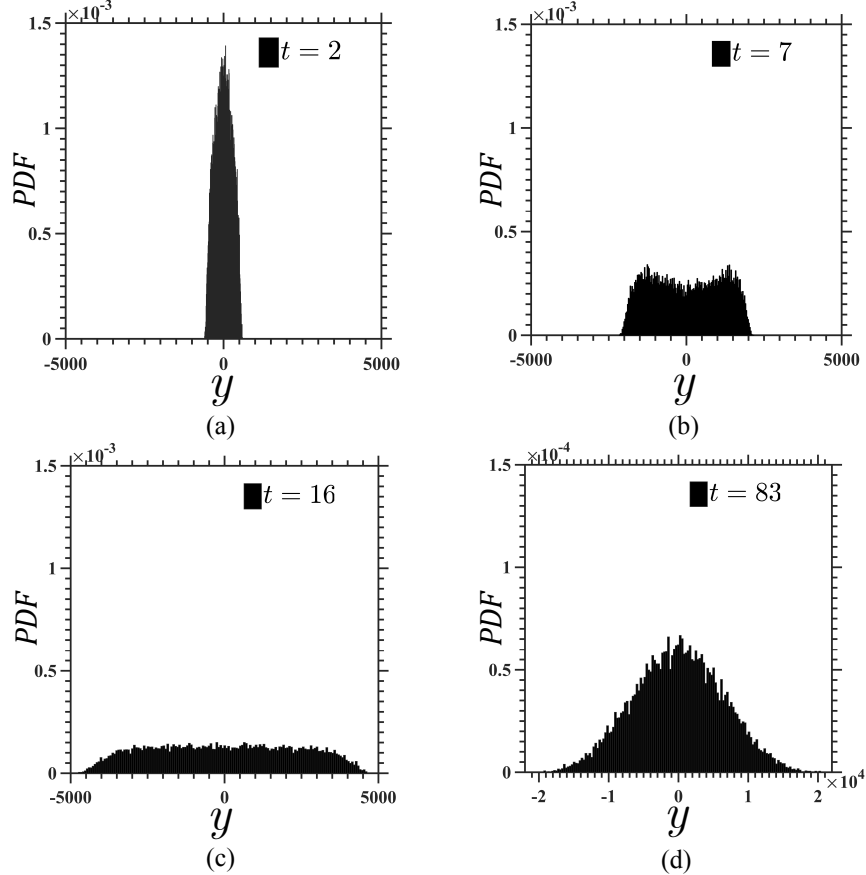


FIG. 7. Probability distributions of the  $y$ -position of a simulated swimmer at different times for  $Pe = 1500$ .

dimensional random walker with the same molecular diffusion coefficient. The reason for the enhancement is that fluctuations in the tilt angle away from  $180^\circ$  lead to a non-zero propulsion force which has a transient persistence in direction before decorrelating. The rapid increase at early times appears in the figure because  $t = 0$  corresponds to the initial state of the simulations, when the particle is placed away from the surface and translates before settling down to its stationary configuration. This behavior is more evident in the plot of the displacement vs. time in Fig. 10b, where the particle translates in the initial  $x$  direction before reaching its equilibrium configuration. In contrast to the skimming case, the probability distributions in  $y$  turn out to be Gaussian at all times.

Decreasing the Péclet number enhances the fluctuations, and for values below 200 the particle tends to leave the wall after a transient period, since the (larger) fluctuations in orientation eventually bring  $\Xi$  below  $90^\circ$  and the particle is driven away, until further fluctuations reorient the particle back towards the wall. A sample trajectory at  $Pe = 100$

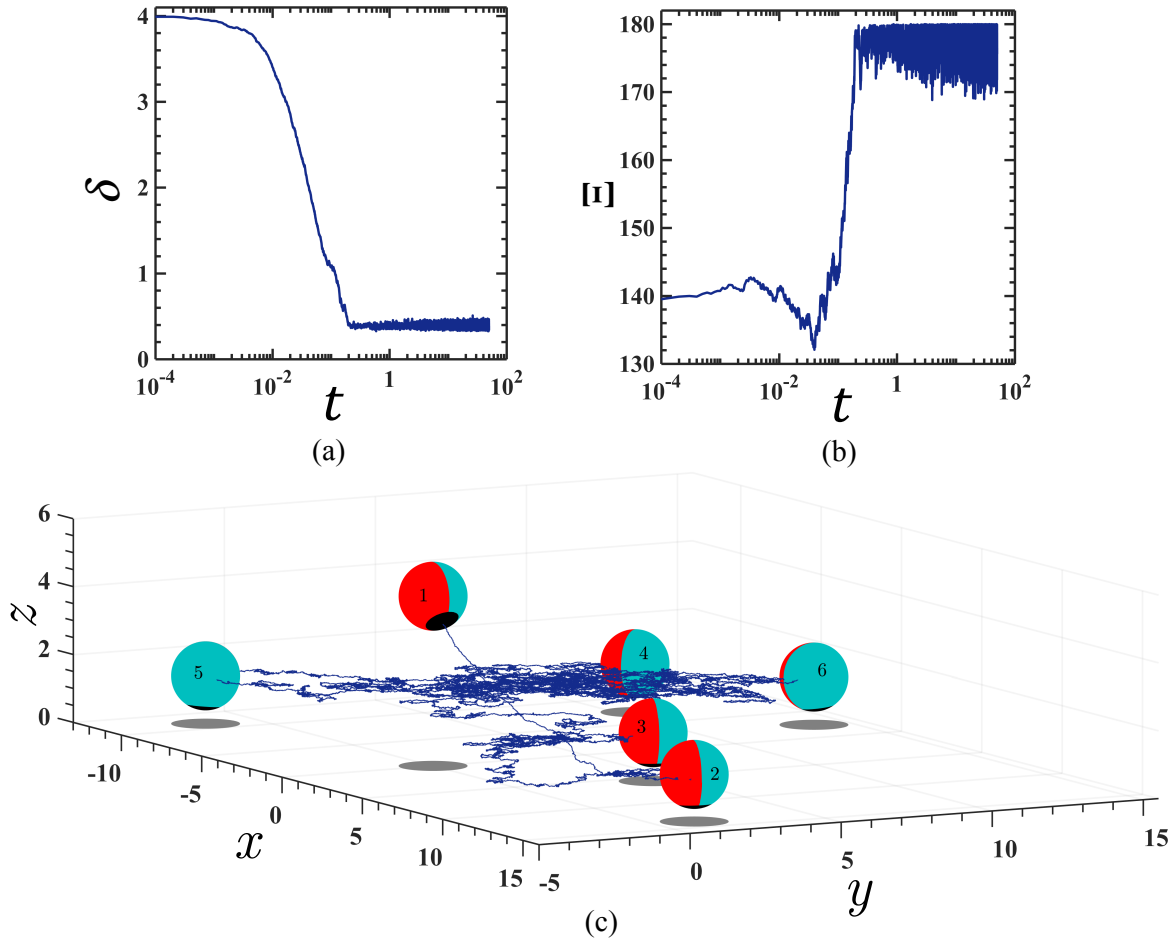


FIG. 8. Example of a swimmer with  $\theta_{cap} = 150^\circ$  and initial configuration  $\delta = 4.0$  and  $\Xi = 140^\circ$  for  $Pe = 1500$ . (a) Variation of separation distance with time, (b) Variation of tilt angle with dimensionless time and (c) A sample trajectory, indicating the orientation.

is shown in Fig. 11, indicating the larger positional fluctuations and the transience of the near-wall state.

#### IV. SUMMARY AND CONCLUSION

This paper has studied the effect of thermal noise on the motion of a diffusiophoretically self-propelled colloid near a no-slip planar wall that does not adsorb solute. We focus on a spherical Janus swimmer with a symmetric catalytic cap as a model engine which autonomously moves in the fluid medium. The mechanism driving the motion of the colloid is neutral self-diffusiophoresis where uncharged solutes with repulsive interactions are pro-

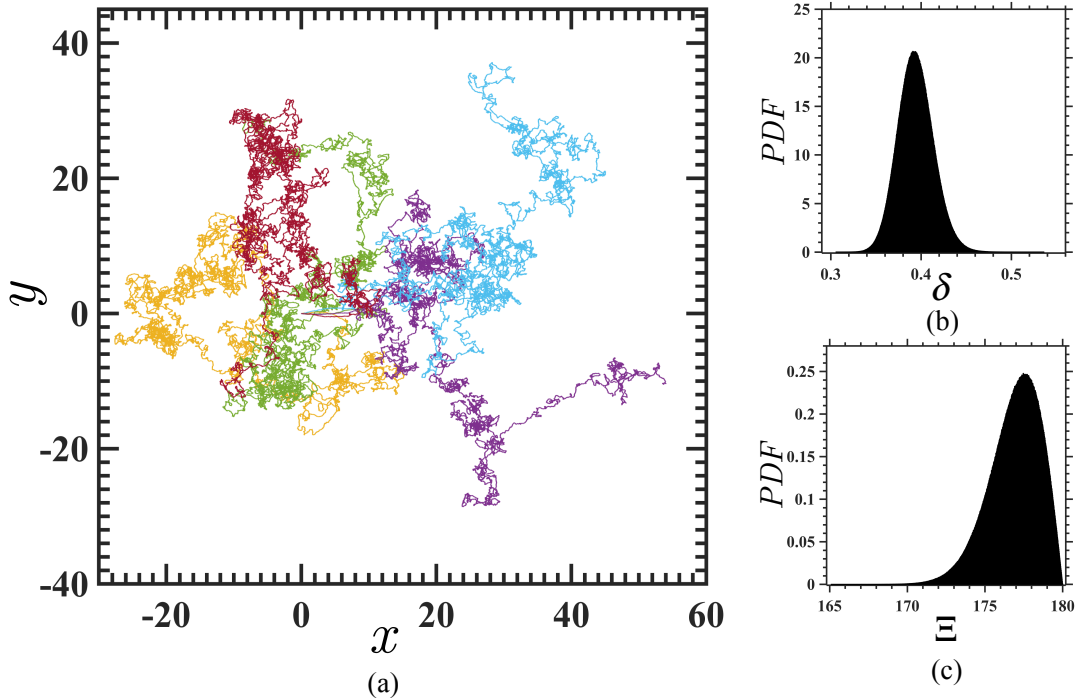


FIG. 9. Swimmers at  $Pe = 1500$  with initial condition  $\delta = 4.0$  and  $\Xi = 140^\circ$  (a) Projection of trajectories in the  $x$ - $y$  plane for five realization, (b) PDF of gap distance and (c) PDF of inclination angle.

duced with constant flux at active cap of the particle. Moreover, the thin interaction-layer limit is assumed, which allows us to formulate the mass transfer and hydrodynamics of the problem based on a slip velocity approach. In this treatment, the gradient of the solute along the surface of the swimmer (arising from the asymmetry of activity at the surface of the particle) creates a force on the fluid in the interaction zone which varies tangentially along the surface and is balanced by fluid pressure outside the interaction layer. This pressure gradient produces a slip velocity tangent to the particle surface towards the catalytic cap and propels the colloid in the opposite direction, at least in the absence of any boundaries. It has been shown previously that in the deterministic limit a nearby planar wall can drastically change the rectilinear motion of a Janus swimmer, and for particles with high active coverages skimming and stationary states of motion can arise when the active side faces away from the wall. A linear stability analysis shows that these states are stable for small translational and rotational perturbations of the particle. A particularly relevant perturbation for colloidal particles arises from thermal fluctuations in the liquid, and we have investigated their consequences for skimming and stationary swimmers within

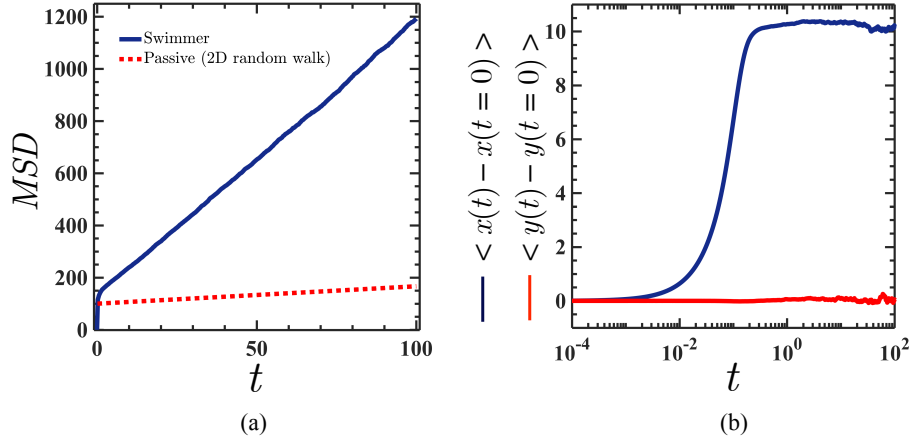


FIG. 10. Swimmer at  $Pe = 1500$  approaching the stationary configuration. (a) In-plane mean square displacement vs. time for the swimmer (solid line) compared to a passive 2d random walker (dashed line), (b) average displacement along  $x$  and  $y$  axis as a function of time.

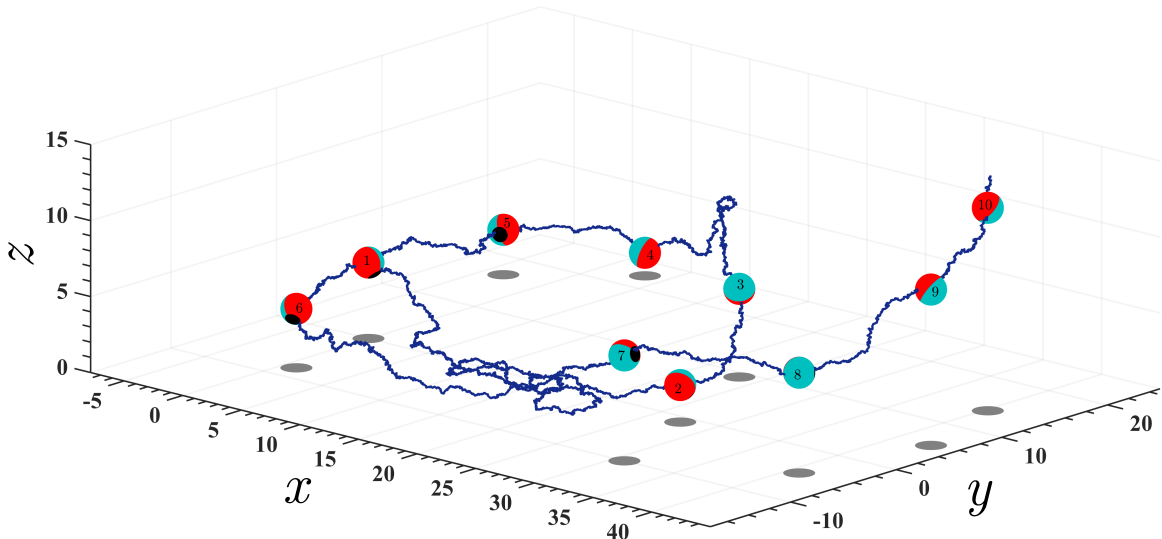


FIG. 11. Trajectory of swimmer with  $\theta_{cap} = 150^\circ$  for small values of Péclet number  $Pe = 100$ .

a Brownian dynamics framework. At large values of the Péclet number, when the propulsive force dominates thermal forces, the skimming states persist with the particle gliding along the wall with small fluctuations in tilt angle and separation distance from the wall, with the averages peaked around the deterministic values. Likewise, at high  $Pe$  the stationary swimmer remains trapped near the wall, with orientation close to normal, where the dominant fluctuations are rotation around the axis normal to the wall and lateral motion along the wall. The strength of the fluctuations increase as the Péclet number falls, so that

the skimming and stationary states becomes transient, and at very low Péclet the motion becomes unpredictable. For the skimmer, the transition from ballistic to diffusive motion occurs at times much larger than the rotational diffusion time, where memory of the initial orientation is completely lost, and also exhibits some transient initial non-Gaussian behavior in its positional fluctuations. The stationary swimmer does not show directed motion and remains in the Gaussian regime at times, and the particle has a larger diffusivity than a passive particle diffusing near a wall. The principal conclusion of the paper is thus that the skimming and stationary states are robust, and can provide a platform for applications.

## V. APPENDIX 1

We require the torque on a sphere in the presence of a planar wall, rotating about an axis normal to the wall, with boundary conditions of no-slip on the surface of the sphere and the wall. Due to the reversibility of the Stokes equations the force on the particle vanishes and the torque is in the normal direction. This problem was first solved by Jeffrey<sup>42</sup> using the fundamental solution of Laplace's equation in bispherical coordinates, and from this we can express the correction to hydrodynamic torque relative to that of particle freely rotating in an infinite medium as

$$f_{\perp}^{rr} \equiv \frac{T_z}{8\pi\mu a^3\Omega} = \sinh^2 \beta_0 \sum_{n=1}^{\infty} n(n+1) \frac{e^{-(n+\frac{3}{2})\beta_0} - e^{-(n-\frac{1}{2})\beta_0}}{\sinh(n+\frac{1}{2})\beta_0}, \quad (22)$$

where  $\Omega$  is the angular velocity and  $\beta_0 = \cosh^{-1}(\delta + 1)$ . This expression was obtained previously by Lee and Leal<sup>43</sup> for a particle rotating near a planar fluid-fluid interface.

## VI. APPENDIX 2

We wish to compare the behavior of the orientational correlation function for diffusing swimmer in two and three dimensions. The direction unity vector  $\hat{\mathbf{u}}$  satisfies the rotational diffusion equation, and the corresponding Greens' function is

$$G_3(\hat{\mathbf{u}}, t; \hat{\mathbf{u}}_0, 0) = \sum_{l=0}^{\infty} \sum_{m=-l}^l e^{-Dl(l+1)t} Y_{lm}(\theta, \phi) Y_{lm}^*(\theta_0, \phi_0),$$

in three dimensions, where  $D$  is the diffusivity and  $\theta$  and  $\phi$  are the spherical coordinate angles associated with  $\hat{\mathbf{u}}$ , and

$$G_2(\hat{\mathbf{u}}, t; \hat{\mathbf{u}}_0, 0) = \sum_{l=-\infty}^{\infty} e^{-Dl^2 t} \frac{1}{\sqrt{2\pi}} e^{-il\phi} \frac{1}{\sqrt{2\pi}} e^{+il\phi},$$

in two dimensions, where  $\phi$  is the polar coordinate angle of  $\hat{\mathbf{u}}$  and  $1/\sqrt{2\pi} \exp(-il\phi)$  is the normalized eigenfunction. The probability distribution for  $\hat{\mathbf{u}}$  is given by in either case by

$$P(\hat{\mathbf{u}}, t) = \int d\hat{\mathbf{u}}_0 G(\hat{\mathbf{u}}, t; \hat{\mathbf{u}}_0, 0) P_0(\hat{\mathbf{u}}_0),$$

where  $P_0$  is the distribution of initial orientations. The correlation function of interest is  $C(t) = \langle \hat{\mathbf{u}}(t) \cdot \hat{\mathbf{u}}(0) \rangle$  and the integral over  $\hat{\mathbf{u}}(0)$  selects out the  $l = 1$  term, which has a time dependance  $e^{-2Dt}$  in three dimensions and  $e^{-Dt}$  in two.

## REFERENCES

- <sup>1</sup>S. Ebbens and J. Howse, “In pursuit of propulsion at the nanoscale,” *Soft Matter* **6**, 726–738 (2010).
- <sup>2</sup>W. Poon, “From clarkia to escherichia and janus: The physics of natural and synthetic active colloids,” *Proceedings of the International School of Physics “Enrico Fermi”, Course CLXXXIV “Physics of Complex Colloid”*, eds. C. Bechinger, F. Sciortino and P. Zihlerl, IOS, Amsterdam: SIF, Bologna , 317–386 (2013).
- <sup>3</sup>S. Ebbens, “Active colloids: Progress and challenges towards realising autonomous applications,” *Current Opinion in Colloid & Interface Science* **21**, 14–23 (2016).
- <sup>4</sup>S. Campuzano, D. Kagan, J. Orozco, and J. Wang, “Motion-driven sensing and biosensing using electrochemically propelled nanomotors,” *Analyst* **136**, 4621–4630 (2011).
- <sup>5</sup>W. Wang, W. Duan, S. Ahmed, A. Sen, and T. Mallouk, “From one to many: Dynamic assembly and collective behavior of self-propelled colloidal motors,” *Acc. Chem. Res.* **48**, 1938–1946 (2015).
- <sup>6</sup>M. Guix, C. Mayorga-Martinez, and A. Merkoçi, “Nano/micromotors in (bio) chemical science applications,” *Chem. Rev.* **114**, 6285–6322 (2014).
- <sup>7</sup>W. Duan, W. Wang, S. Das, V. Yadav, T. Mallouk, and A. Sen, “Synthetic nano-and micromachines in analytical chemistry: Sensing, migration, capture, delivery, and separation,” *Annu. Rev. Anal. Chem.* **8**, 311–333 (2015).
- <sup>8</sup>J. Anderson, “Colloid transport by interfacial forces,” *Annu. Rev. Fluid Mech.* **21**, 61–99 (1989).
- <sup>9</sup>J. Howse, R. Jones, A. Ryan, T. Gough, R. Vafabakhsh, and R. Golestanian, “Self-motile colloidal particles: from directed propulsion to random walk,” *Phys. Rev. Lett.* **99**, 048102 (2007).
- <sup>10</sup>V. Yadav, W. Duan, P. Butler, and A. Sen, “Anatomy of nanoscale propulsion,” *Annu. Rev. Biophys.* **44**, 77–100 (2015).
- <sup>11</sup>J. Anderson, M. Lowell, and D. Prieve, “Motion of a particle generated by chemical gradients part 1. non-electrolytes,” *J. Fluid Mech.* **117**, 107–121 (1982).
- <sup>12</sup>M. Popescu, M. Tasinkevych, and S. Dietrich, “Pulling and pushing a cargo with a catalytically active carrier,” *Euro. Phys. Lett.* **95**, 28004 (2011).

- <sup>13</sup>N. Sharifi-Mood, A. Mozaffari, and U. Córdova-Figueroa, “Pair interaction of catalytically active colloids: from assembly to escape,” *J. Fluid Mech.* **798**, 910–954 (2016).
- <sup>14</sup>S. Michelin and E. Lauga, “Autophoretic locomotion from geometric asymmetry,” *Eur. Phys. J. E* **38**, 1–16 (2015).
- <sup>15</sup>S. Shklyaev, J. Brady, and U. Córdova-Figueroa, “Non-spherical osmotic motor: chemical sailing,” *J. Fluid Mech.* **748**, 488–520 (2014).
- <sup>16</sup>S. Michelin and E. Lauga, “Phoretic self-propulsion at finite pécelet numbers,” *J. Fluid Mech.* **747**, 572–604 (2014).
- <sup>17</sup>E. Yariv and S. Michelin, “Phoretic self-propulsion at large pécelet numbers,” *J. Fluid Mech.* **768**, R1 (2015).
- <sup>18</sup>A. Frankel and A. Khair, “Dynamics of a self-diffusiophoretic particle in shear flow,” *Phys. Rev. E* **90**, 013030 (2014).
- <sup>19</sup>G. Volpe, I. Buttinoni, D. Vogt, H. Kümmerer, and C. Bechinger, “Microswimmers in patterned environments,” *Soft Matter* **7**, 8810–8815 (2011).
- <sup>20</sup>C. Kreuter, U. Siems, P. Nielaba, P. Leiderer, and A. Erbe, “Transport phenomena and dynamics of externally and self-propelled colloids in confined geometry,” *Eur. Phys. J. Spec. Top.* **222**, 2923–2939 (2013).
- <sup>21</sup>S. Das, A. Garg, A. I. Campbell, J. Howse, A. Sen, D. Velegol, R. Golestanian, and S. Ebbens, “Boundaries can steer active janus spheres,” *Nat. Commun.* **6**, 8999 (2015).
- <sup>22</sup>J. Simmchen, J. Katuri, W. Uspal, M. Popescu, M. Tasinkevych, and S. Sánchez, “Topographical pathways guide chemical microswimmers,” *Nat. Commun.* **7**, 10598 (2016).
- <sup>23</sup>D. Crowdy, “Wall effects on self-diffusiophoretic janus particles: a theoretical study,” *J. Fluid Mech.* **735**, 473–498 (2013).
- <sup>24</sup>Y. Ibrahim and T. Liverpool, “The dynamics of a self-phoretic janus swimmer near a wall,” *Euro. Phys. Lett.* **111**, 48008 (2015).
- <sup>25</sup>W. Uspal, M. Popescu, S. Dietrich, and M. Tasinkevych, “Self-propulsion of a catalytically active particle near a planar wall: from reflection to sliding and hovering,” *Soft matter* **11**, 434–438 (2015).
- <sup>26</sup>A. Mozaffari, N. Sharifi-Mood, J. Koplik, and C. Maldarelli, “Self-diffusiophoretic colloidal propulsion near a solid boundary,” *Physics of Fluids* **28**, 053107 (2016).
- <sup>27</sup>F. Yang, S. Qian, Y. Zhao, and R. Qiao, “Self-diffusiophoresis of janus catalytic micro-motors in confined geometries,” *Langmuir* **32**, 5580–5592 (2016).

- <sup>28</sup>P. Romanczuk, M. Bär, W. Ebeling, B. Lindner, and L. Schimansky-Geier, “Active brownian particles,” *Eur. Phys. J. Spec. Top.* **202**, 1–162 (2012).
- <sup>29</sup>A. Zöttl and H. Stark, “Emergent behavior in active colloids,” *J. Phys. Condens. Matter* **28**, 253001 (2016).
- <sup>30</sup>C. Bechinger, R. Di Leonardo, H. Löwen, C. Reichhardt, G. Volpe, and G. Volpe, “Active brownian particles in complex and crowded environments,” arXiv preprint arXiv:1602.00081 (2016).
- <sup>31</sup>B. ten Hagen, S. van Teeffelen, and H. Löwen, “Brownian motion of a self-propelled particle,” *J. Phys. Condens. Matter* **23**, 194119 (2011).
- <sup>32</sup>A. Kaiser, H. Wensink, and H. Löwen, “How to capture active particles,” *Phys. Rev. Lett.* **108**, 268307 (2012).
- <sup>33</sup>D. Takagi, J. Palacci, A. Braunschweig, M. Shelley, and J. Zhang, “Hydrodynamic capture of microswimmers into sphere-bound orbits,” *Soft Matter* **10**, 1784–1789 (2014).
- <sup>34</sup>S. Spagnolie, G. Moreno-Flores, D. Bartolo, and E. Lauga, “Geometric capture and escape of a microswimmer colliding with an obstacle,” *Soft Matter* **11**, 3396–3411 (2015).
- <sup>35</sup>A. Brown, I. Vladescu, A. Dawson, T. Vissers, J. Schwarz-Linek, J. Lintuvuori, and W. Poon, “Swimming in a crystal,” *Soft matter* **12**, 131–140 (2016).
- <sup>36</sup>K. Schaar, A. Zöttl, and H. Stark, “Detention times of microswimmers close to surfaces: influence of hydrodynamic interactions and noise,” *Phys. Rev. Lett.* **115**, 038101 (2015).
- <sup>37</sup>D. Ermak and J. McCammon, “Brownian dynamics with hydrodynamic interactions,” *J. Chem. Phys.* **69**, 1352–1360 (1978).
- <sup>38</sup>J. Brady and G. Bossis, “Stokesian dynamics,” *Annu. Rev. Fluid Mech.* **20**, 111–157 (1988).
- <sup>39</sup>C. Bender and S. Orszag, *Advanced mathematical methods for scientists and engineers* (McGraw-Hill Book Company, New York, USA, 1978).
- <sup>40</sup>D. Beard and T. Schlick, “Unbiased rotational moves for rigid-body dynamics,” *Biophys. J.* **85**, 2973–2976 (2003).
- <sup>41</sup>A. Lau and T. Lubensky, “State-dependent diffusion: Thermodynamic consistency and its path integral formulation,” *Phys. Rev. E* **76**, 011123 (2007).
- <sup>42</sup>G. Jeffery, “On the steady rotation of a solid of revolution in a viscous fluid,” *Proc. R. Soc. A* **2**, 327–338 (1915).
- <sup>43</sup>S. Lee and L. Leal, “Motion of a sphere in the presence of a plane interface. part 2. an exact solution in bipolar co-ordinates,” *J. Fluid Mech.* **98**, 193–224 (1980).